NASA/TM–20230006677

CALPHAD Models to Guide Refractory Alloys Additive Manufacturing: In-Situ Compounds Formation, Nanoparticles, and Impurities Considerations

F.N. Michael and J.W. Sowards
Marshall Space Flight Center, Huntsville, Alabama

May 2023

The NASA STI Program…in Profile

The NASA STI Program collects, organizes, provides for archiving, and disseminates NASA's STI. The NASA STI program provides access to the NTRS Registered and its public interface, the NASA Technical Reports Server, thus providing one of the largest collections of aeronautical and space science STI in the world. Results are published in both non-NASA channels and by NASA in the NASA STI Report Series, which includes the following report types:

• TECHNICAL PUBLICATION. Reports of completed research or a major significant phase of research that present the results of NASA programs and include extensive data or theoretical analysis. Includes compilations of significant scientific and technical data and information deemed to be of continuing reference value. NASA's counterpart of peer-reviewed formal professional papers but has less stringent limitations on manuscript length and extent of graphic presentations.

• TECHNICAL MEMORANDUM. Scientific and technical findings that are preliminary or of specialized interest, e.g., quick release reports, working papers, and bibliographies that contain minimal annotation. Does not contain extensive analysis.

• CONTRACTOR REPORT. Scientific and technical findings by NASA-sponsored contractors and grantees.

• CONFERENCE PUBLICATION. Collected papers from scientific and technical conferences, symposia, seminars, or other meetings sponsored or cosponsored by NASA.

• SPECIAL PUBLICATION. Scientific, technical, or historical information from NASA programs, projects, and mission, often concerned with subjects having substantial public interest.

• TECHNICAL TRANSLATION. English-language translations of foreign scientific and technical material pertinent to NASA's mission.

Specialized services also include organizing and publishing research results, distributing specialized research announcements and feeds, providing information desk and personal search support, and enabling data exchange services.

For more information about the NASA STI program, see the following:

• Access the NASA STI program home page at http://www.sti.nasa.gov

• Help desk contact information:

https://www.sti.nasa.gov/sti-contact-form/ and select the "General" help request type.

NASA/TM–20230006677

CALPHAD Models to Guide Refractory Alloys Additive Manufacturing: In-Situ Compounds Formation, Nanoparticles, and Impurities Considerations

F.N. Michael and J.W. Sowards
Marshall Space Flight Center, Huntsville, Alabama

May 2023

TRADEMARKS

TABLE OF CONTENTS

LIST OF FIGURES

LIST OF FIGURES (Continued)

LIST OF ACRONYMS, ABBREVIATIONS, AND SYMBOLS

Al   aluminum

AM   additive manufacturing

ARC   Ames Research Center

BCC   body-centered cubic

C   carbon

CALPHAD   Calculation of Phase Diagrams

CSC   crack susceptibility coefficient

DBTT   ductile-to-brittle transition temperature

DED   directed energy deposition

DFT   density functional theory

DICTRA   Diffusion Module

GRC   Glenn Research Center

H   hydrogen

HfC   hafnium carbide

ICME   integrated computational materials engineering

MC   metal carbide

MO   metal oxide

Mo   molybdenum

MSFC   Marshall Space Flight Center

O   oxygen

LIST OF ACRONYMS, ABBREVIATIONS, AND SYMBOLS (continued)

OD	oxide dispersoid
PBF	powder bed fusion
ppm	parts per million
RAAMBO	refractory alloy additive manufacturing build optimization
Re	rhenium
SLM	selective laser melting
SNP	Space Nuclear Propulsion
SLS	Space Launch System
TaC	tantalum carbide
Ta	tantalum
TDB	thermodynamic database
TM	technical memorandum
W	tungsten
wt.%	weight percent

NOMENCLATURE

f_s	fraction of solid
T	temperature

TECHNICAL MEMORANDUM

CALPHAD MODELS TO GUIDE REFRACTORY ALLOYS ADDITIVE MANUFACTURING: IN-SITU COMPOUNDS FORMATION, NANOPARTICLES, AND IMPURITIES CONSIDERATIONS

1. INTRODUCTION

An as-yet unpublished article from the authors details an integrated computational materials engineering (ICME) model for Rosenthal analytical melt pool selective laser melting (SLM), as well as Thermo-Calc®'s Diffusion Module (DICTRA)[1] diffusion kinetics models for the same laser beam-induced melt pool temperatures and dynamics. These models capture the effects of various temperatures on refractory metals and their alloys and on nanometer-scale particle, or 'nanoparticle,' inclusions of metal carbide (MC). Two conclusions arose from analysis of these models:

(1) A static or dynamic feedback control of melt pool temperatures below nanoparticle inclusion melt temperature, yet above the refractory alloy melt temperature, would assure particle survival and preserve the effectiveness of the inclusions as simultaneous strength and ductility enhancers even after solidification, through grain refinement and thermal stability via Zener pinning; and

(2) Exceeding such temperatures would melt the nanoparticle inclusions into an equivalent elementally dispersed, or 'diffused,' weight percent (wt.%) composition addition to the system. Any subsequent in-situ formation or alloying of precipitated nanoparticle MC and/or metal oxide (MO) inclusions would proceed from there.

Based on these insights, this technical memorandum (TM) seeks to model and discuss aspects of nanoparticle and micrometer-scale particle or 'microparticle' inclusions in refractory metal alloy manufacturing, via a currently used additive manufacturing (AM) method that results in equivalent wt.% addition of dissolved elements in the melt pool composition and subsequent formation of nanometer-scale MC and MO inclusions. Additionally, the authors begin to consider the effects of oxygen (O), a ubiquitous impurity, in AM; and seek to understand a combined optimization of alloying, nano- and micro strengthening and refinement, elemental additions, and even in-situ compounds and alloys species formation. To gain insights, this TM focuses on a pair of refractory alloys currently of interest to NASA: tungsten-rhenium-tantalum carbide (with O impurities) (W-Re-TaC(-O)) and tungsten-rhenium-tantalum-carbon (with O impurities) (W-Re-Ta-C(-O)), which are processed via powder bed fusion (PBF)-SLM.

2. BACKGROUND

Ultra-high-temperature operational environments exist for many aerospace applications that NASA has an interest in advancing and deploying. These include hypersonic aircraft, space nuclear propulsion (SNP), chemical propulsion components (e.g., nozzles and liners) such as those found on the Space Launch System (SLS), and re-entry vehicles, to name a few.

Various NASA Centers and external partners are showing great interest in high-temperature, high-strength propulsion components. NASA and partners are using these components in increasingly cross-disciplinary and coordinated partnerships for multiple projects, including the Refractory Alloy Additive Manufacturing Build Optimization (RAAMBO) multi-Center project led by NASA Marshall Space Flight Center (MSFC) and including NASA Ames Research Center (ARC) and NASA Glenn Research Center (GRC); the SNP project, also led by MSFC in conjunction with the U.S. Department of Energy (DOE) laboratories; and the prime SLS/Artemis project.

Refractory metals and their alloys are high-temperature-tolerant materials that are of great utility in high-temperature applications, if the manufacturing processes of joining (e.g., welding and AM) can be perfected. Refractory metals and their alloys exhibit several features that make the optimization of manufacturing refractories challenging. These include high ductile-brittle transition temperatures (DBTTs);[2,3] susceptibility to impurity-derived embrittlement and cracking, such as from hydrogen (H) and O; solidification cracking; and even high neutron absorption cross sections for various elemental additions, as well as high cost in creating refractory alloy compositions.[4]

Currently, three routes to refractory metals-based manufacturing are under investigation at NASA Centers. These include sintering approaches, PBF-SLM, and directed energy deposition (DED). In addition, joining built parts and generally refractory components via welding is also under investigation.[5–7]

3. DISCUSSION

The focus of this TM is the computational modeling of W-Re-TaC and W-Re-Ta-C (both with and without consideration of O impurities) and the manufacturing thereof via PBF-SLM, with a focus on the melt pool dynamics under two limiting melt temperature regimes.

In an SLM process, melt pool temperatures are very high in order to melt the refractory metal and elements used to alloy. These temperatures exceed the base metals' melt temperatures and often are much higher, with reported temperatures reaching approximately 4,500–6,000 K.[8–13] The build chamber(s) are mostly operated with an inert gas flow, although vacuum can be utilized. Impurities such as O are continuously removed or reacted, such as by a partial H gas flow in addition to the inert gas, in order to react and scavenge O. Note that there are two possible O sources: (1) from the environment, and (2) from the refractory metal and added elements in the form of MOs, which may have embedded O impurities.

Various atomic elements are added to the pre-melt, typically in the form of powders. These elements are added to suppress solidification cracking and to cool down hot cracking; and to impart certain properties to the refractory alloy such as increased strength, increased ductility, corrosion resistance, surface roughness, or other thermal and/or mechanical attributes. These usually result in some desirable properties; however, for most refractory alloys, a trade-off between enhanced strength and enhanced ductility has been perceived to exist. That is, strength can be increased at the expense of a lowered ductility, and conversely, ductility can be increased at the expense of a lowered strength.

However, an additional non-chemistry-based modification approach exists,[9,10] ideally resulting in a simultaneous strength and ductility improvement. This approach utilizes the addition of nanometer-scale particles, or 'nanoparticles,' to the micrometer-scale particles, or 'microparticles,' in the alloy composition. If these nanoparticles remain unmelted, one of three outcomes can occur depending on their size:

(1) Nanoparticles can be engulfed in the solidifying grain, acting as a strengthener (if below a critical radius, depending on the size of the base materials and the process being used).

(2) Nanoparticles can be pushed along the solidification front to reside in grain boundaries and grain vertices, acting as Zener grain pinning effectors and potentially imparting strength even under a wide thermal operational range (i.e., thermal stability).

(3) Nanoparticles can act as nucleation sites during solidification, ensuring fine grains and moving the alloy away from columnar and dendritic growth and toward equiaxed grain growth.

Equiaxed grain growth results in a strengthening effect via grain refinement, as well as a ductility enhancement via the creation of fine grain boundaries' many tortuous paths, which

prevent easy initiated crack propagation. Yet the high temperature of the manufacturing process's melt pool remains an obstacle to optimally implementing such a strategy to ensure equiaxed grain growth. Note that in the case of lightweight alloys with a low melt temperature, such as aluminum (Al) and its alloys with a ≈940 K melt temperature, additions of nanoparticles such as TaC with a melt temperature of ≈4,100 K allows for an extremely wide temperature window of ≈3,160 K for ensuring the survivability of unmelted nanoparticles. In the case of a refractory base metal such as W with a melt temperature of ≈3,700 K, this window shrinks to merely ≈400 K. As a result, it is more difficult to implement a similar strategy via control of the melt pool temperature. This is by design, because PBF-SLM uses a static dialed-in laser power that generates a consistent volumetric energy density and surface energy density.

Additionally, the selection of higher-melting particle additions such as TaC or hafnium carbide (HfC) with its ≈4,200 K melt temperature, or even carbon nanotubes and graphene flakes with >4,500 K melt temperatures, over other MCs with lower melt temperatures nearer to that of W may theoretically allow for—or even expand—that manufacturing window in conjunction with the W-alloy liquidus depression from pure W;[10] even as fine-tuned melt pool temperature control, such as with a two-color pyrometer real-time feedback control, may ensure a tightly stable and controlled melt pool temperature within a window. While this latter temperature control approach has been demonstrated in the laboratory for PBF-SLM by academia, the technology has not yet been incorporated in the current state of the art equipment utilized by NASA and industry partners for either process development or manufacturing.

Another consideration is relevant then to the melting of nanoparticles. In the example of W, a powder mix of refractory metal and nanoparticles (e.g., W-TaC, comprised of 100 μm powdered W coated with 50 nm TaC nanoparticles) will fully melt if the melt pool is in the reported ranges above and will behave identically to an elemental composition such as W-Ta-C.

This issue is still present in the case of elemental additions to the base refractory metal in order to modify chemistry and properties. For example, and as relevant to this TM, the addition of Re to W is a route to enhancing ductility in W.[4] The mechanisms for this so-called 'rhenium effect' are explained in various ways. On the crystal lattice level, these include the Re-induced formation of an additional <112> slip planes in addition to the body-centered cubic (BCC) <110> primary or base metal's lattice's minimal slip planes even at low temperatures. These additional slip planes contribute to the activation of screw dislocation glide transition softening. In addition, alloying a softer (i.e., relatively lower yield strength) elemental material to the harder elemental primary base metal material in this case results in a softening effect in the near equal atomic radius substitutional input into the primary lattice of the harder element (W) by the softer element (Re), with a reduction of the stress fields experienced and an overall lowered energy for activation of slip. Thirdly, the chemistry of the melt pool now experiences various undercooling and supercooling effects due to concentration gradients of the Re in W and the dendritic and columnar solidification initiated in pure W. These cooling effects cause changes to granular boundary formation that also cause changes in scale, in temperature ranges for initiation and fragmentation, and even in the resultant grain sizes of formed (final) grains. The change in size of these formed (final) grains then modifies their morphology and, in the specific case of (final) primary grains, their average diameter under various process laser parameters, thus leading to conclusions of a grain refining effect—though

4

this last effect is only on a small scale. That is, the grain refinement due to elemental (chemical) additions are smaller in scale and are limited to effects on the micrometer scale; while, for example, nanoparticles that remain intact and which act as nucleation sites themselves result in so-called 'ultra' grain refinement to the sub-micron and even nanometer scales.

The melt pool environment itself will drive various in-situ stoichiometric and non-stoichiometric compounds formation, which often are discussed in terms of alloys formation. Given an elemental composition, various species and phases can result, and many will result given the solidification environment. An issue here, which has been the subject of previous unpublished research from the authors and from which the insights have been applied in this TM, is that in the case of a fully melted nanoparticle, the diffused particle's composition will not re-coalesce into a nanoparticle of a preferred size and shape or one that resembles the initial nanoparticle. If any particle is formed at all, it will form very small-scale dispersoids, typically between 1–10 nm in diameter.[13] Also, depending on the solubility of the melted elements, some of the dissolved elements of the nanoparticle inclusions will embed interstitially or substitutionally in the base element. The diffused element will embed substitutionally if the atomic radius ratio is within ≈1.6 of the base element; otherwise, the diffused element will embed interstitially. This is seen in how smaller carbon atoms will embed interstitially in larger iron atoms in the creation of carbon steel. In the case of the alloys discussed in this TM, the Re will incorporate substitutionally into the primary lattice of the base W, as the large Re atoms will simply not electromagnetically 'fit' in the spaces between the planes of W atoms.

Therefore, in the case of laser-induced high melt pool temperatures, a system with diffused elements from nanoparticles becomes equivalent to a system composed of the individual elements. In the case discussed in this TM, the W-Re-TaC system with fully diffused TaC nanoparticles will behave identically or near-identically to a W-Re-Ta-C system. This 'near-identical' caveat depends on the thermal gradient of the melt pool and peak temperature, and even re-scans and hatching, as it can be imagined that some very thin layer of the more viscous melt may contain thermal gradients and temperature distributions that may be below the nanoparticle's melt temperatures, which may then cause nanoparticles to escape full diffusion. However, this ideal situation is unlikely to occur.

Furthermore, new or re-alloying in-situ dynamics will occur depending on the elements present in addition to the nanoparticle's elements. Moreover, the presence of ubiquitous impurities such as oxygen will add further complexity and even create challenges to assuring a crack free solidified part, as in-situ formation of MOs will also occur in addition to MCs and the expected alloys from the base metal plus elements added. Note that O solubility in a solid refractory metal such as W is poor. As the laser source moves away and the melt pool begins to cool and solidify, O will either be ejected or driven toward the remaining melt, eventually resulting in an O concentration increase in the remaining melt and the formation of various MO species at grain boundaries. Therefore, potentially embrittling MO species may result exactly where the most heightened vulnerability to cracking and crack propagation can occur (i.e., along grain boundaries). This issue has been discussed in the authors' unpublished research and is being restated here; the authors include detailed Calculation of Phase Diagrams (CALPHAD)-based computations that attempt to take this issue into account in section 3.2.

Yet even this detrimental outcome via impurities may present opportunities for favorable utilization. A type of particle known as an oxide dispersoid (OD) is known to enhance strength and ductility in AM of various metal alloys.[9] Though some ODs may contribute to embrittling depending on their shape and size, ODs added to a high-melt-temperature melt pool will diffuse entirely into their constituent elements. This diffusion destroys the previous sizing and shape of the ODs, and upon solidification of the melt pool, its previous pinning effects. However, in-situ formation of fine-scale dispersed ODs can be a strategy to reduce the embrittling effect of O. Adding certain wt.% of various elements into the alloy allows them to act as so-called 'getters' of O impurities, such as the addition of C resulting in carbon monoxide (CO) vapor, which can be expelled and flow-removed by the entraining inert gas mixture. The addition of various elements of metals with a higher affinity than W for binding with O can also result in the in-situ formation of MOs that then will act favorably as ODs in the built part or will form MO regions of cells or grains themselves. Note, however, that as is the case with MCs, there also are temperature limits to these formed ODs. A typical upper limit is near or below the melting temperature of W, indicating that in a refractory such as W, the usual MO particle addition will nearly always melt. With solid state high temperature stability (below solidus temperature), the ODs in the built part will have less thermal stability than the added or in-situ formed (and re-formed at small scale) MCs.

In order to characterize and predictively model these effects and considerations, in an effort to overcome some of the primary challenges in the AM builds of refractory alloys, section 3.2 discusses various modeling approaches and considerations that have been selected as being relevant. Each problem as been reduced to its components and various aspects have been modeled. The authors utilize these models to both gain insight and to provide guidance for the synergistic ICME approach being applied to RAAMBO, SNP and similar ultra-high temperature aerospace applications at NASA.

3.1 Recap of the Melt Pool Rosenthal Analytical Model and the Thermo-Calc Diffusion Module Model

In as-yet unpublished research, the authors utilized a melt pool Rosenthal moving heat source analytical solutions to the heat equation to predict melt pool behavior when a laser traversed W metal. The melt pool was also modeled via Thermo-Calc DICTRA diffusion kinetics.[1] The examples discussed in the research concluded that a 100-nm diameter TaC dispersoid/inoculant nanoparticle is likely to be completely consumed in a 3D print of W with relevant laser processing parameters. The time scales of the full melts at the melt temperatures and laser powers considered for those elements ranged from ≈10^{-6} s to ≈10^{-9} s depending on the model and assumptions, even while the typical PBF build parameters showed that the melt region exposure of the particles (i.e., the exposure times above melting points) were on the scale of 0.13 ms or ≈10^{-4} s. The work provided insight and suggested a methodology for this CALPHAD work that the authors use in this TM to model the refractory alloy systems of interest of W-Re-TaC and W-Re-Ta-C with and without O impurities.

6

3.2 Discussion of Models and Results

This section seeks to deconstruct the problem into its component parts and build more complexity and degrees of freedom via additional elements. The initial model starts with the base W-Re system, as shown in figure 1. The Thermo-Calc Scheil solidification calculation, the property model calculations, and phase diagram calculations are applied to the system. Note the very high gradient at >0.9 fraction of solid (f_s), which is indicative of extremely high thermal strains near solidus.
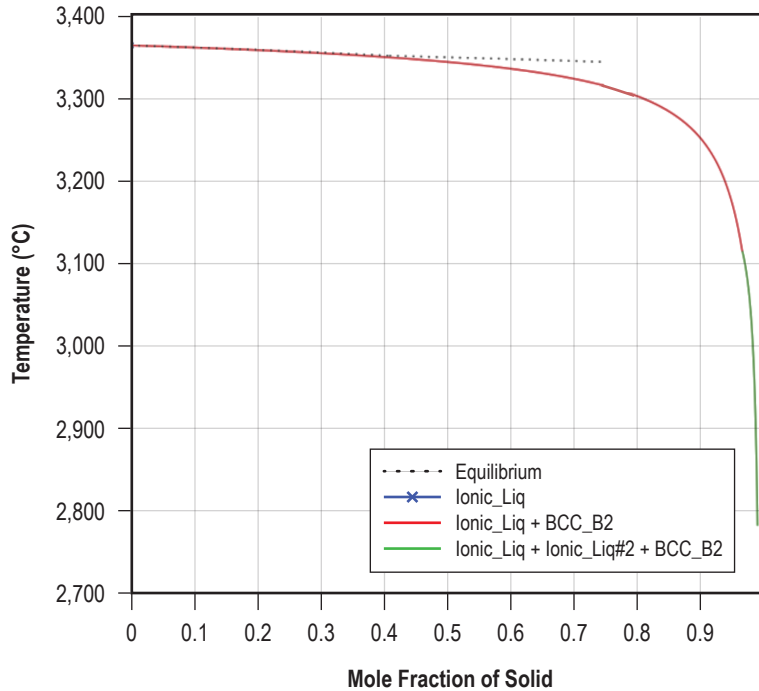

Figure 1. Thermo-Calc classical Scheil solidification calculation of the base W-Re system. The Re composition is 5.5 wt.% and all other elemental impurities are <0.01 wt.%.

Figure 2a shows the crack susceptibility coefficient (CSC) according to Thermo-Calc for the W-Re system with varied Re wt.% compositions. The CSC corresponds to the ratio of time spent vulnerable to cracking compared to time spent invulnerable to cracking during solidification. A typical PBF-SLM print as discussed in section 3 has two potential sources of O impurities: from the ambient air in the chamber and from the powder feedstock. Assuming that inert gas with H partial pressure and outflow removes the O impurities from the ambient air in the chamber, the majority of O impurities will be from the powder itself. Various reported sensor data have reported O ranges of 5–250 parts per million (ppm), with one known instance of 750 ppm. The models therefore are adapted to include O in these ranges, calculating the relative amount of O to be ≈0.01–0.2 wt.%. Figure 2b shows the CSC for a W-Re-O system with 1,000 ppm or 0.1 wt.% O impurity in the melt pool (and not in the build chamber, as measured by O sensors). The CSC for the W-Re-O system is at least an order of magnitude higher for the proposed 5.5 wt.% Re than in the W-Re system with no impurities.
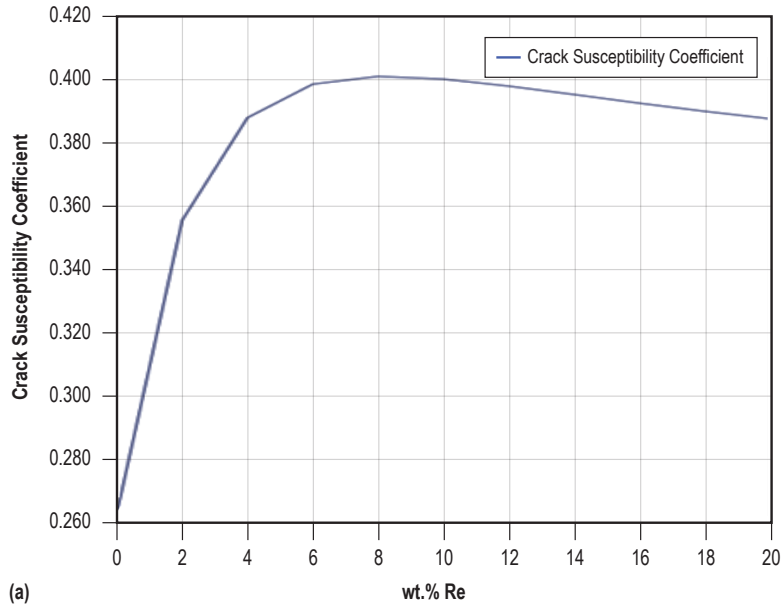
(a)
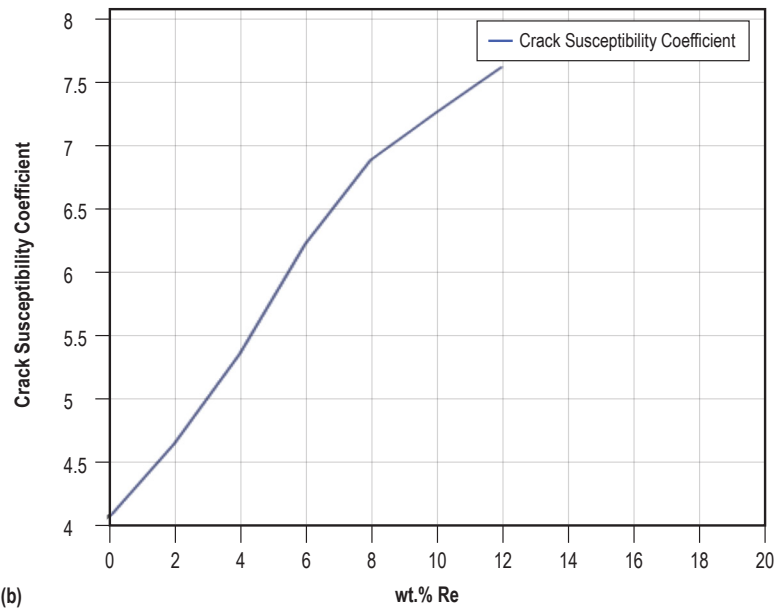
(b)

Figure 2. (a) W-Re crack susceptibility coefficient (CSC) for varied Re wt.% compositions without impurities; (b) W-Re-O system CSC with 1,000 ppm or 0.1 wt% oxygen impurity in the melt pool (and not in the build chamber as measured by O sensors).

The Nickel alloy thermodynamic database (TDB) is also utilized, which contains evaluated O interactions.[14] The High Entropy Alloys database is applied to check several refractory alloys without O interactions in order to corroborate results.[14] The phase diagram for O inclusion as impacting W is utilized to gauge the Nickel TDB's O inclusion into metals solidification (fig. 3). It was concluded that the refractory-oxygen thermodynamics are sufficiently represented in the Nickel TDB. A W-O phase diagram created by Wendel is included for comparison.[15]
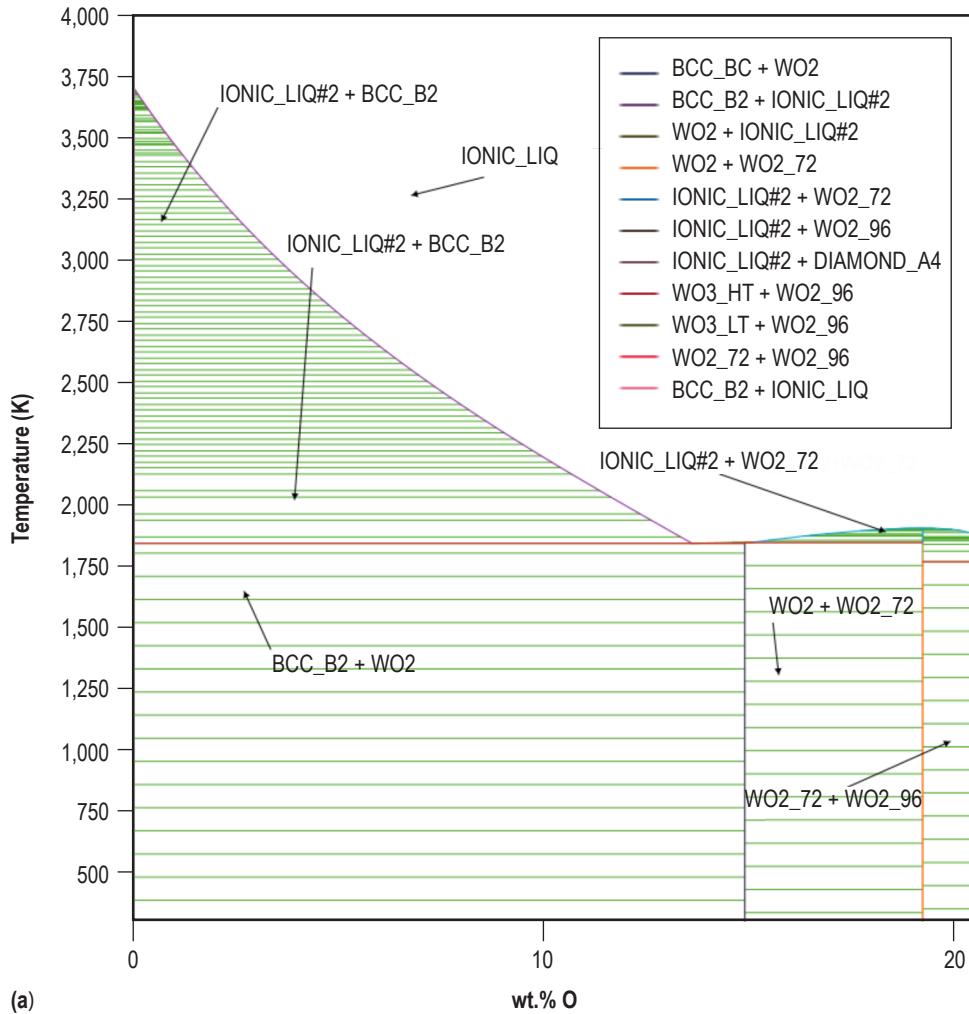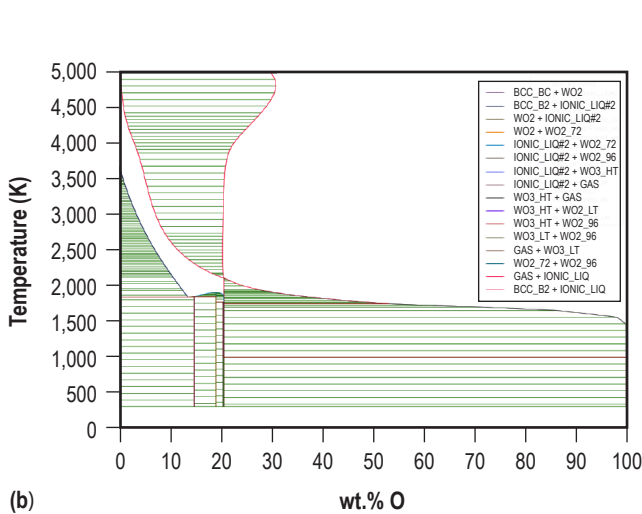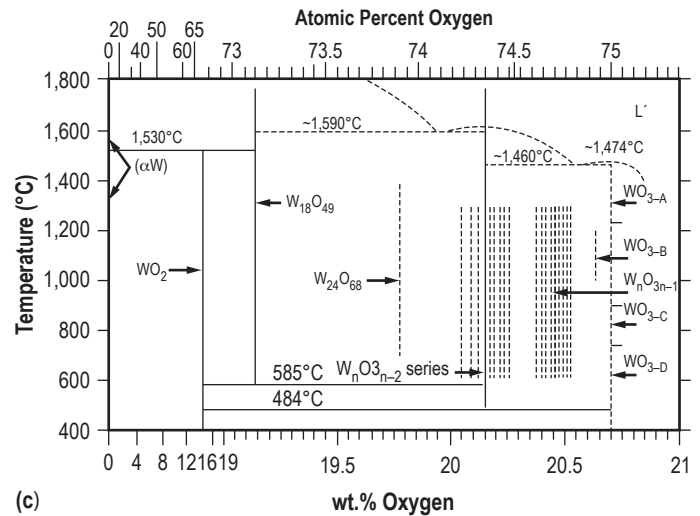
Figure 3. (a) W-O phase diagram in regions of interest; (b) The 'full' W-O diagram, with gas phase and ionic liquid 'on' in the Thermo-Calc modeling; (c) Limited W-O phase diagram for comparison.[15]

A Scheil solidification type of calculation with these W-O wt.% shows minimal variations of the solidification range (i.e., the liquidus-to-solidus temperature differential) in these O ranges, and nor does it flatten the $>0.95\,f_s$ gradient. Note that the steeper the $>0.95\,f_s$ region slope or gradient is, the higher likelihood of solidification cracking to occur. Figure 4 shows the effect of the addition of O in the wt.% range contemplated, which serves to shift the nearly smooth W solidification prior to the $>0.95\,f_s$. However as discussed in section 3, in-situ formation of MOs can occur, especially at the grain boundaries. In figure 4, MOs are shown to emerge beginning at 0.08 wt.% O. However, the formation of MOs such as WO_2 will occur even at lower wt.%'s, as shown in the phase diagram in figure 3. It appears that the Scheil simulation omits to render this formation as the phase being too small in amount-of-phase (i.e., cut-off) at lower O wt.%.
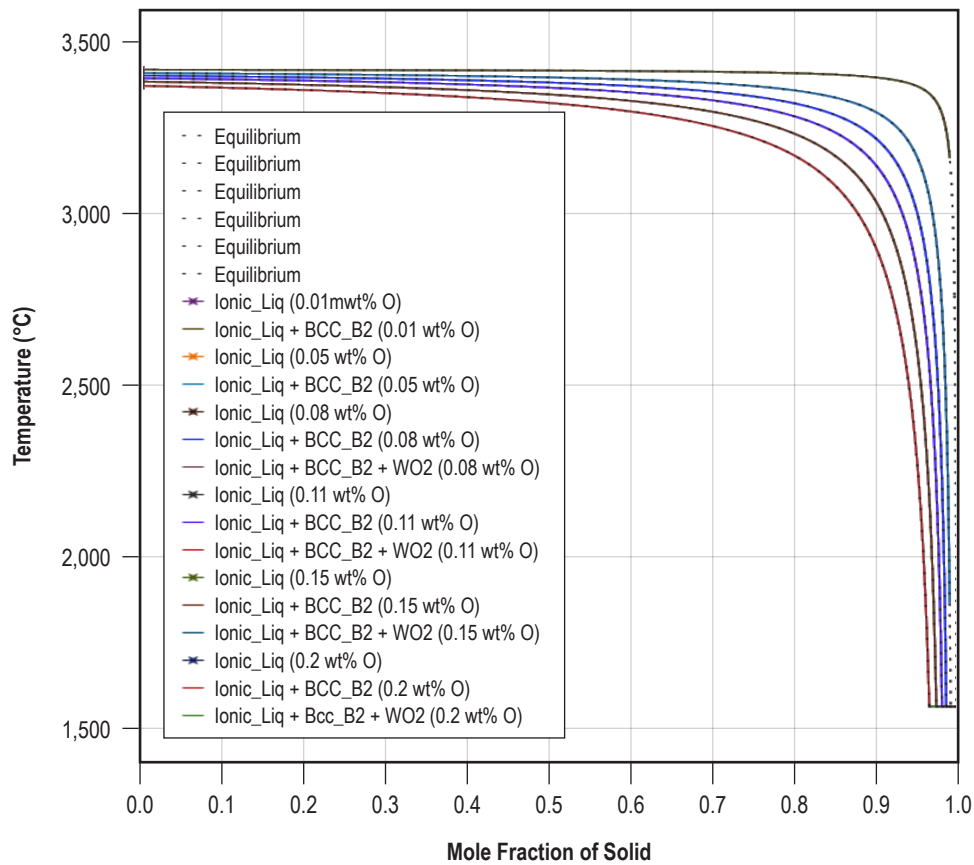

Figure 4. Scheil solidification of W-O at various wt.%. Note the emergence of WO2 at the 0.08 wt.% O level.

The next stage of modeling shows how the addition of C can affect the interaction between W and O. As previously noted, the O wt.% is assumed to be mostly from the powder feedstock source, although some unremoved amounts from the build chamber may yet remain. The C in these models is assumed to be either from the diffusion of MC nanoparticles or from wt.% additions of getter C. The Scheil solidification gradient for this model is shown in figure 5.
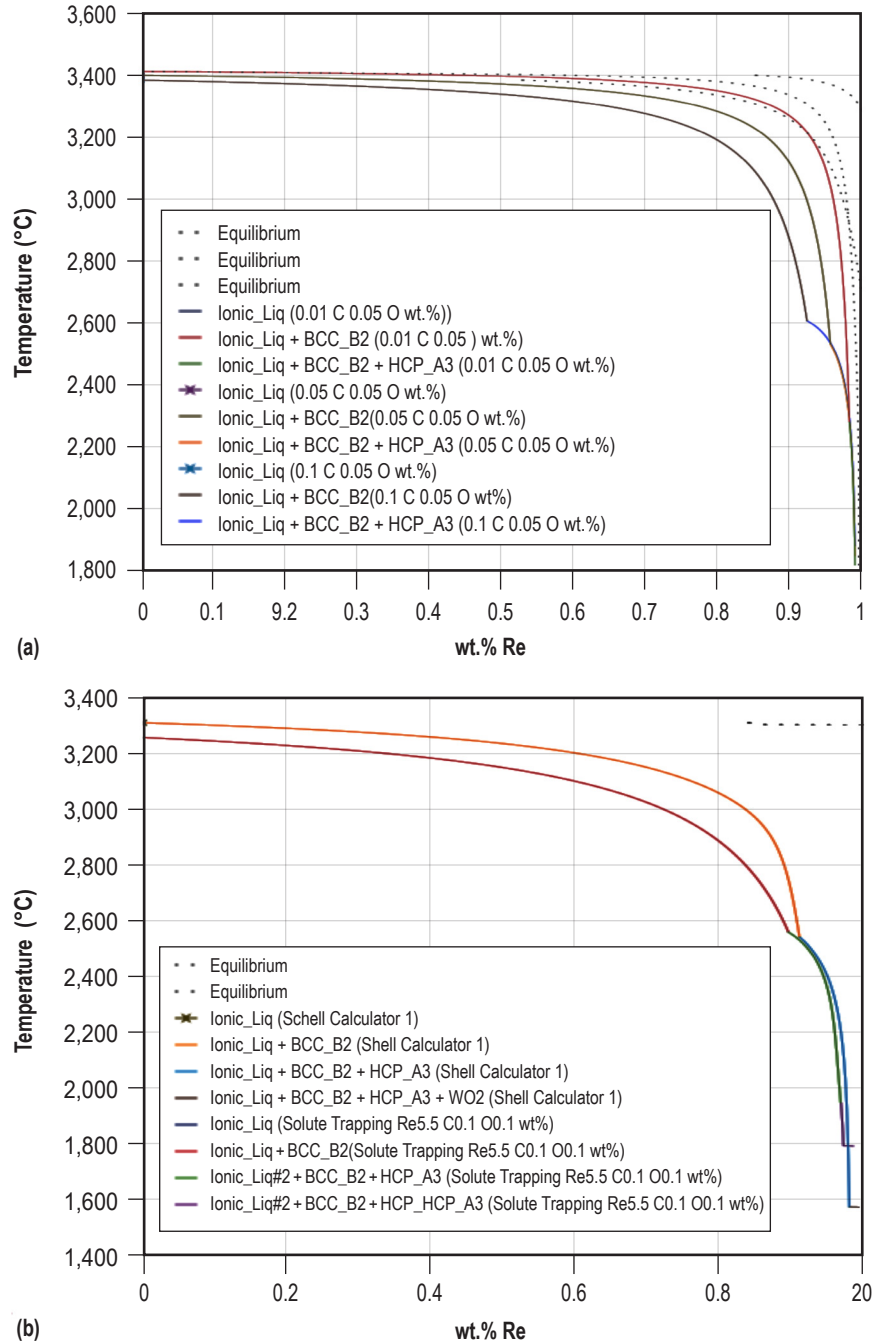
Figure 5. Scheil solidification gradients for (a) W-C-O with various wt.% of C and (b) W-Re-C-O with 5.5 wt.% Re and various wt.% of C and O.

The Thermo-Calc modules allow for a material-to-material calculation to easily vary wt.% of certain materials in a system. Figures 6 and 7 show a W-Re-C-O system with varying amounts of O from 0.01 wt.% to 0.2 wt.%, while keeping wt.% of C and Re constant at 0.1 wt.% and 5.5 wt.%, respectively. The system is evaluated at a stable temperature of 1,000 K in figure 6 and at a temperature range between 500–4,000 K in figure 7. Both figures show stable MC and BCC W formation, with MO formation varying gradually dependent upon the concentration of O.

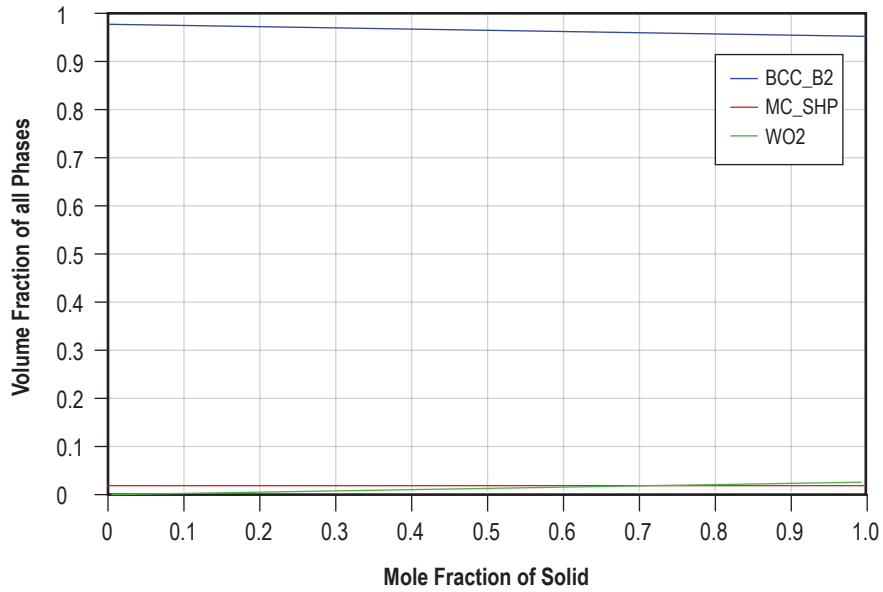| Material Name	Material A	Material B
Composition Re	5.5	5.5
Composition C	0.1	0.1
Composition O	0.01	0.2

Figure 6. W-Re-C-O material-to-material calculation evaluated at 1,000 K.
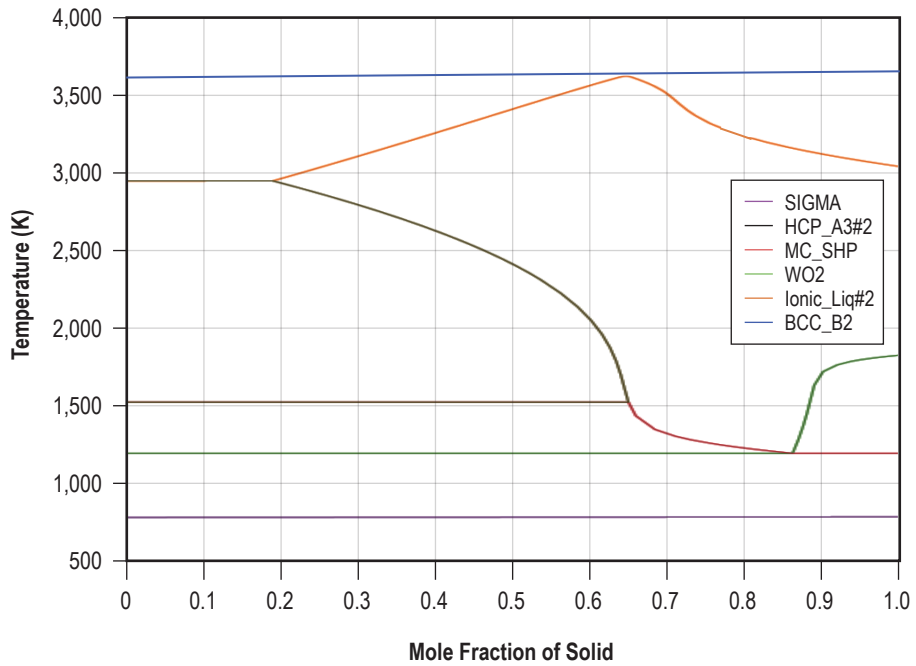

Figure 7. W-Re-C-O material-to-material calculation with temperature variation from 500–4,000 K.

The final step in increasing complexity of the discussed W alloy involves adding Ta to the system. The following calculations explore various aspects of both W-Re-TaC and W-Re-TaC-O, dependent upon whether O impurities are considered or not. If the nanoparticle TaC, with a melting point of ≈4,100 K, is fully melted as a result of high-temperature PBF-SLM, then the calculations explore the systems of W-Re-Ta-C and W-Re-Ta-C-O.

Tantalum as an elemental addition can act as an alloying or binding species to both Re and W, as well as forming MCs and MOs. To illustrate these species, the stable fundamental phases in a W-Re-Ta-C are system are shown schematically in figure 8.[16–18] Note that many of the unstable phases shown in light orange can actually be produced if the environment is such that the formation energy is relatively favorable in the solidification process.
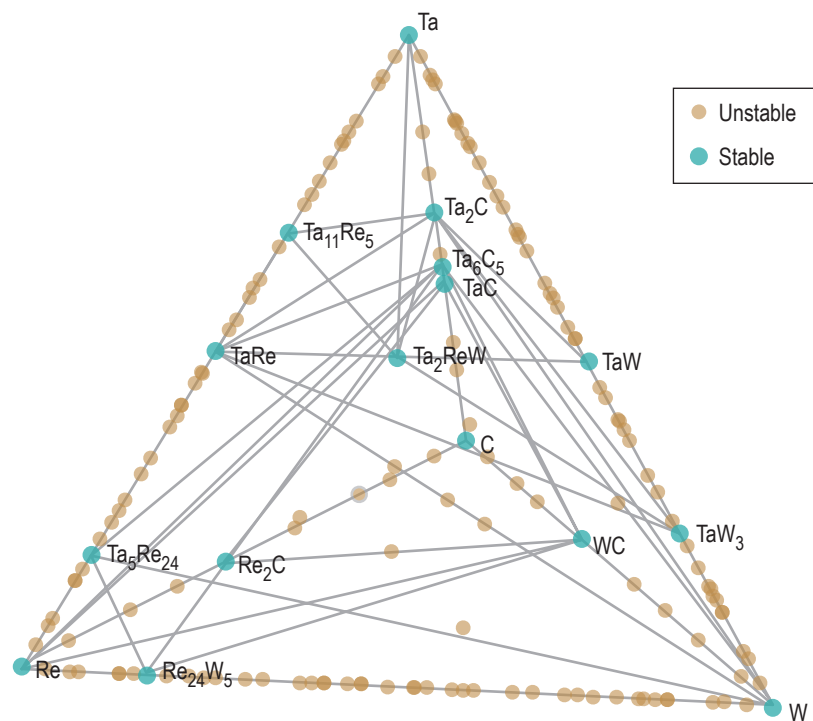

Figure 8. The W-Re-Ta-C 4-species 'pyramid' of stable and unstable interactions.[16–18]

Using density functional theory (DFT), the authors also explore results of interactions of W-Re-Ta-C-O at 0 K to illustrate the potential for Ta to interact with W and Re and not only with C and O. This interaction would not be possible if the TaC nanoparticle inclusion would not have melted, or if the process of AM was within the window between the melting point of W and Re (≈3,600 K) and that of TaC (≈4,100 K). By melting and diffusing TaC into the melt pool, the nanoparticles' many nucleation sites are lost; therefore, the alloy also loses grain ultra-refinement, grain growth suppression, and volume fraction of nanoparticle-dependent Zener pinning at any temperature below solidus. Additional complexity in various phase formations is also introduced into the solidification process.

The addition of Ta in the W-Re-Ta-C-O system to account for fully diffused TaC significantly modifies the Scheil solidification curves as compared to the W-Re-C-O case in figure 5, both in terms of liquidus and solidus temperatures and the steepness of the crucial region at >0.95 f_s. Figures 9–11 show Scheil solidification curves at varying wt.% ratios of Ta and C in W-Re-Ta-C-O systems.
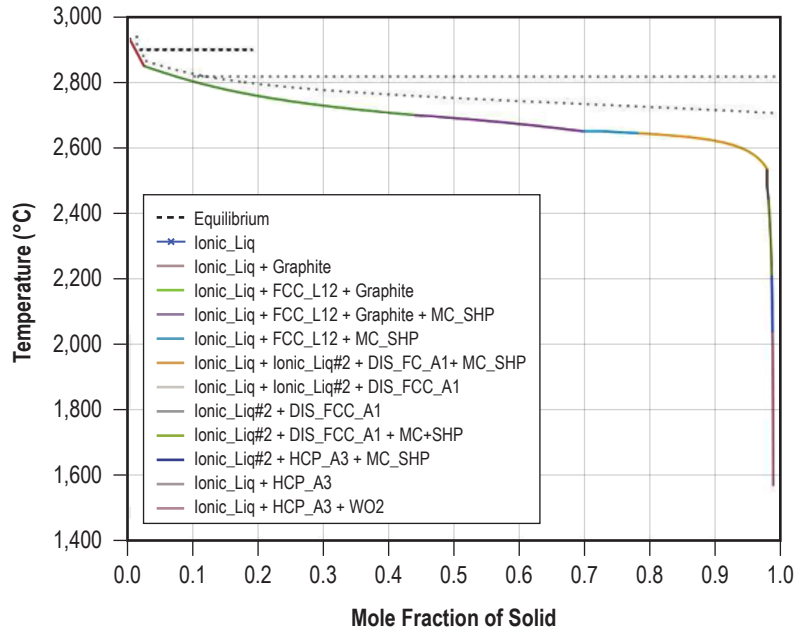

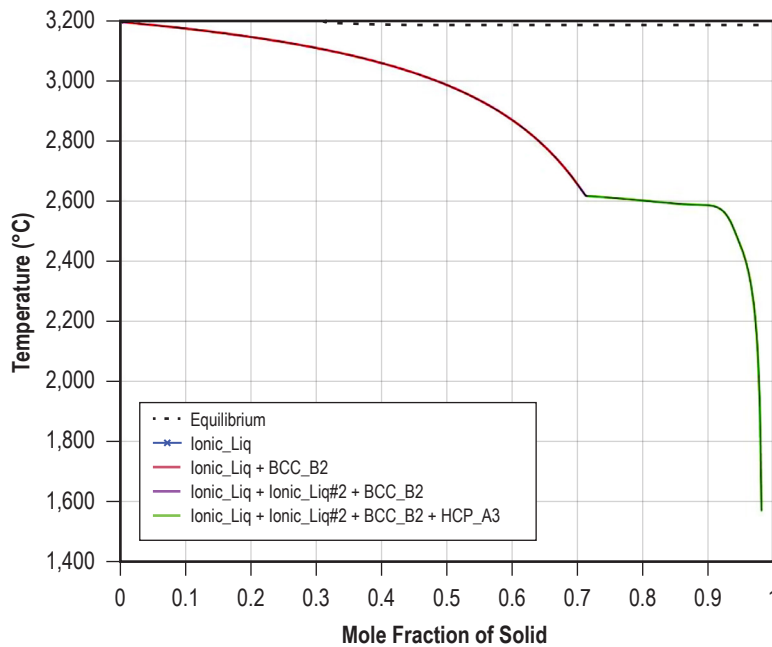Figure 9. W-Re-Ta-C-O at 5.5 wt.% Re, 5 wt.% Ta, 5 wt.% C, and 0.1 wt.% O.

Figure 10. W-Re-Ta-C-O at 5.5 wt.% Re, 0.4 wt.% Ta, 0.4 wt.% C, and 0.1 wt.% O.
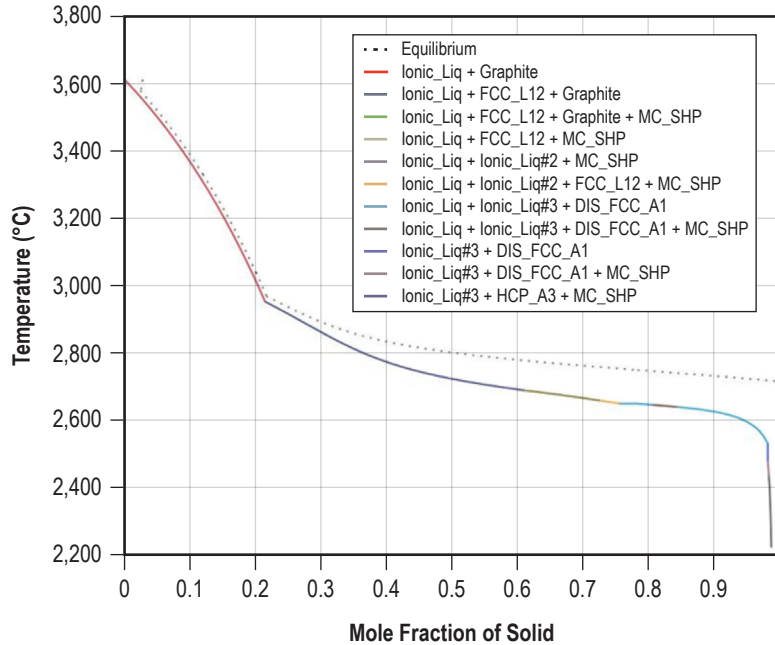
Figure 11. W-Re-Ta-C-O at 5.5 wt.% Re, 8 wt.% Ta, 8 wt.% C, and 0.1 wt.% O.

Note the reduction in steepness of the >0.95 f_s region of solidification, and the temperature range reduction of time spent in the steep region. However, the goal is ultimately to flatten that region for a very gentle curve, which will enable crack-free solidification of AM built parts. The authors intend to revisit this result in other work toward optimization of a crack-free part build and have already predicted various alloy combinations that do exhibit the flattened curve. In addition, the authors are working with NASA partners to further research on PBF-SLM AM manufacturing of such crack-free refractory alloy systems, which will be published in future writings.

Despite the narrowing of the solidification range, the steepness of the slope or gradient of temperature (T) at >0.95 f_s is still high, which is indicative of a susceptibility to cracking. The >0.95 f_s is the hypothetical crucial area for solidification cracking, where the confluence of shrinkage, liquid fraction available to feed voids and spaces between grains, and increase/decrease of strain per region as the f_s approaches 1 is at its most intense.

The authors have investigated the cracking susceptibility via the CSC index available in Thermo-Calc. As before, the research begins with partial components and increases in complexity to the full composition. The amount of Re used in these calculations is centered on 5.5 wt.%, which is added to W in order to impart some grain refinement and mostly to enhance ductility by adding an additional slip system. The CSC index for the system is derived via two methods: the Thermo-Calc vulnerability time method and the Kou-Scheil gradient method, which has recently been published in a separate TM by the authors along with release of the Python module for its use.[19] Both methods are shown in figure 12.
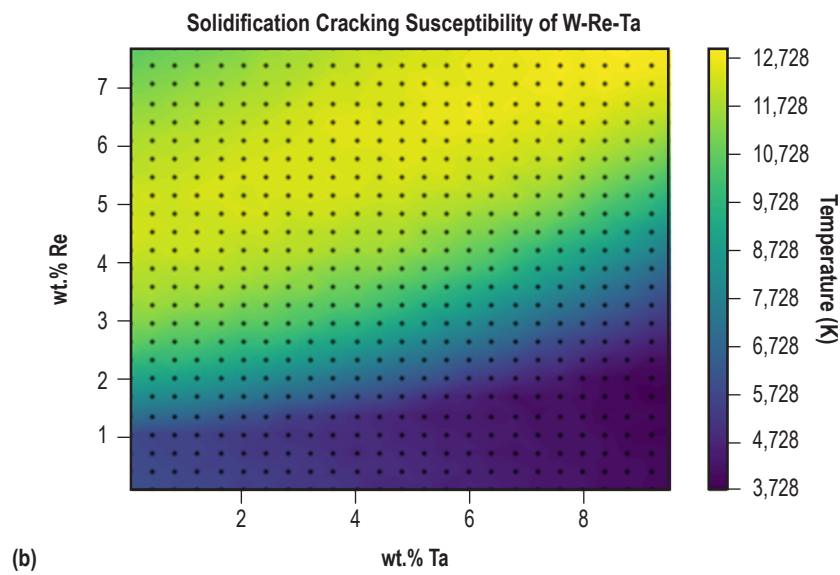
(a)

(b)
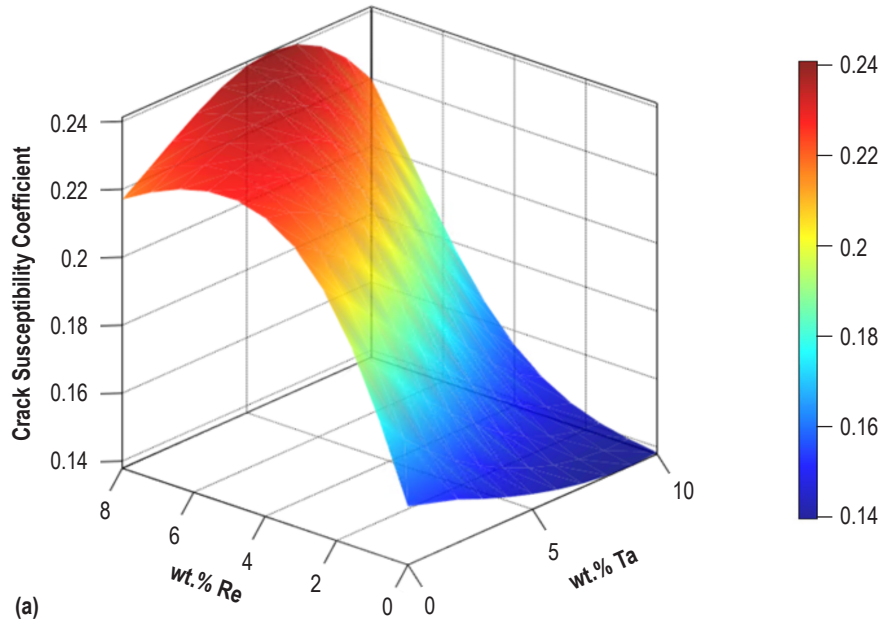
Figure 12. W-Re-Ta-C0.5 CSC index calculated via (a) the Thermo-Calc
vulnerability time method and (b) the Kou-Scheil gradient method.

The two methods are in excellent agreement. Clearly there are windows of low susceptibility, which imply that Re reduction even to the 2 wt.% range imparts ductility while reducing the crack susceptibility.[3] The effects of additional Re are somewhat deleterious in solidification, despite a desirable ductility enhancement and some grain refinement. The present investigation suggests reducing Re while adding Ta to achieve improved properties such as in-situ MC formation. In addition, Ta is a less expensive component compared to Re, providing additional financial benefit.

The addition of C while keeping the amount of Re consistent at 5.5 wt.% also has an effect on suppressing crack susceptibility, which is shown in figure 13:

(a)

(b)

Figure 13. The effect of C addition to the W-Re5.5-Ta-C system where the Ta-C susceptibility to cracking during solidification, as shown in (a) Thermo-Calc vulnerability time method and (B) Kou-Scheil gradient method.
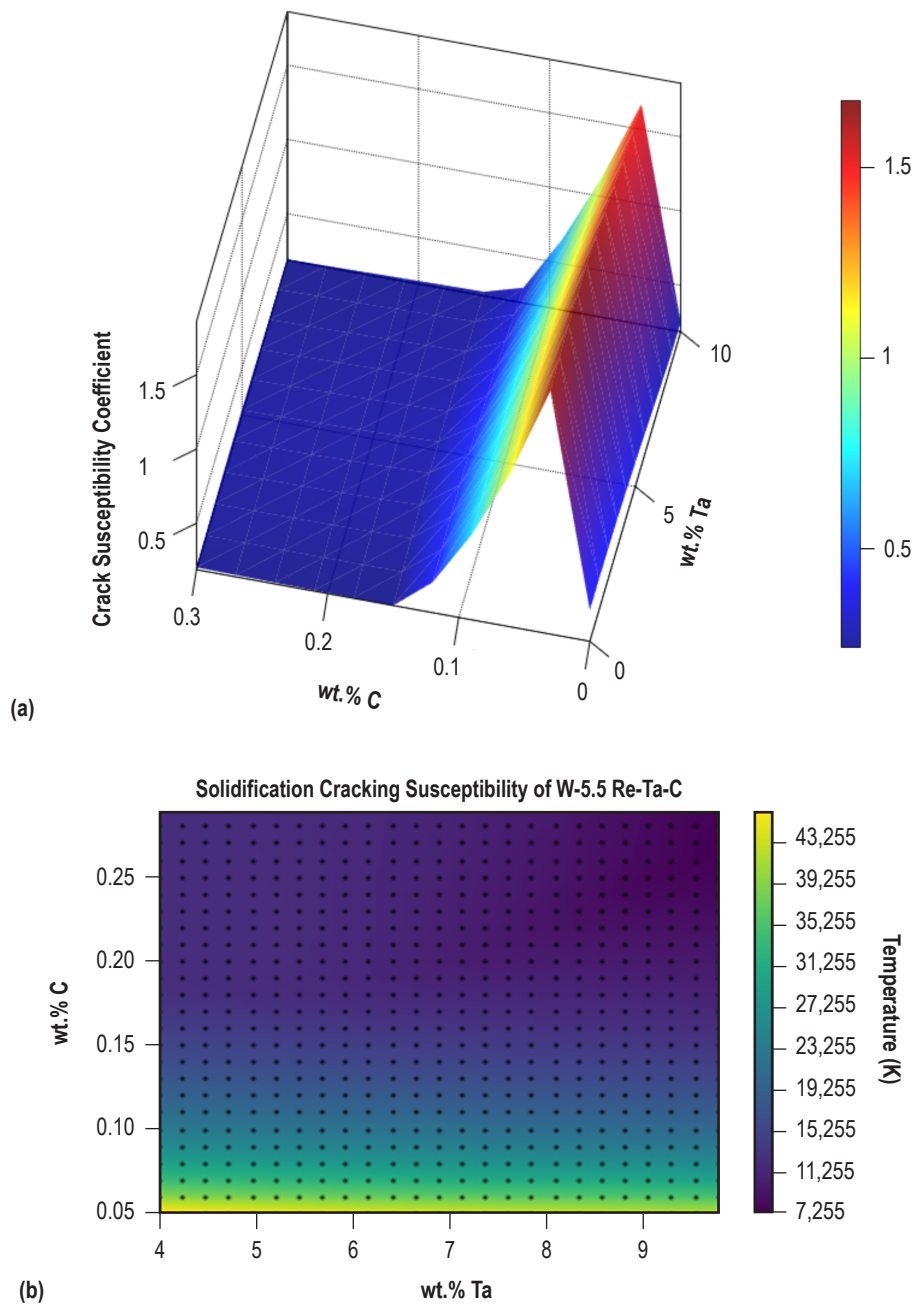
The two methods are in good agreement even at the uneven scaling. In both instances, a suggested improvement and window for improvement via additional C wt.% is noted. The C alloying potential for crack suppression is clearly noticeable in Figs. 12 and 13. In fact, an even higher C wt.% than shown in figure 13 has been found to be a useful addition for crack suppression in refractory alloys AM and in solidification in general, which the authors will discuss in more detail in a follow up TM. Here, it suffices to discuss the effects of Ta-C on the W-Re alloy under investigation and to gain insight on paths forward.

The Effects of O impurities as impacting the W-Re-Ta-C system is also useful to analyze as well, providing feedback into the insights being gained on C and Ta additions. Figure 14 shows CSC indices for different combinations of wt.% ratios within the W-Re-Ta-C system:
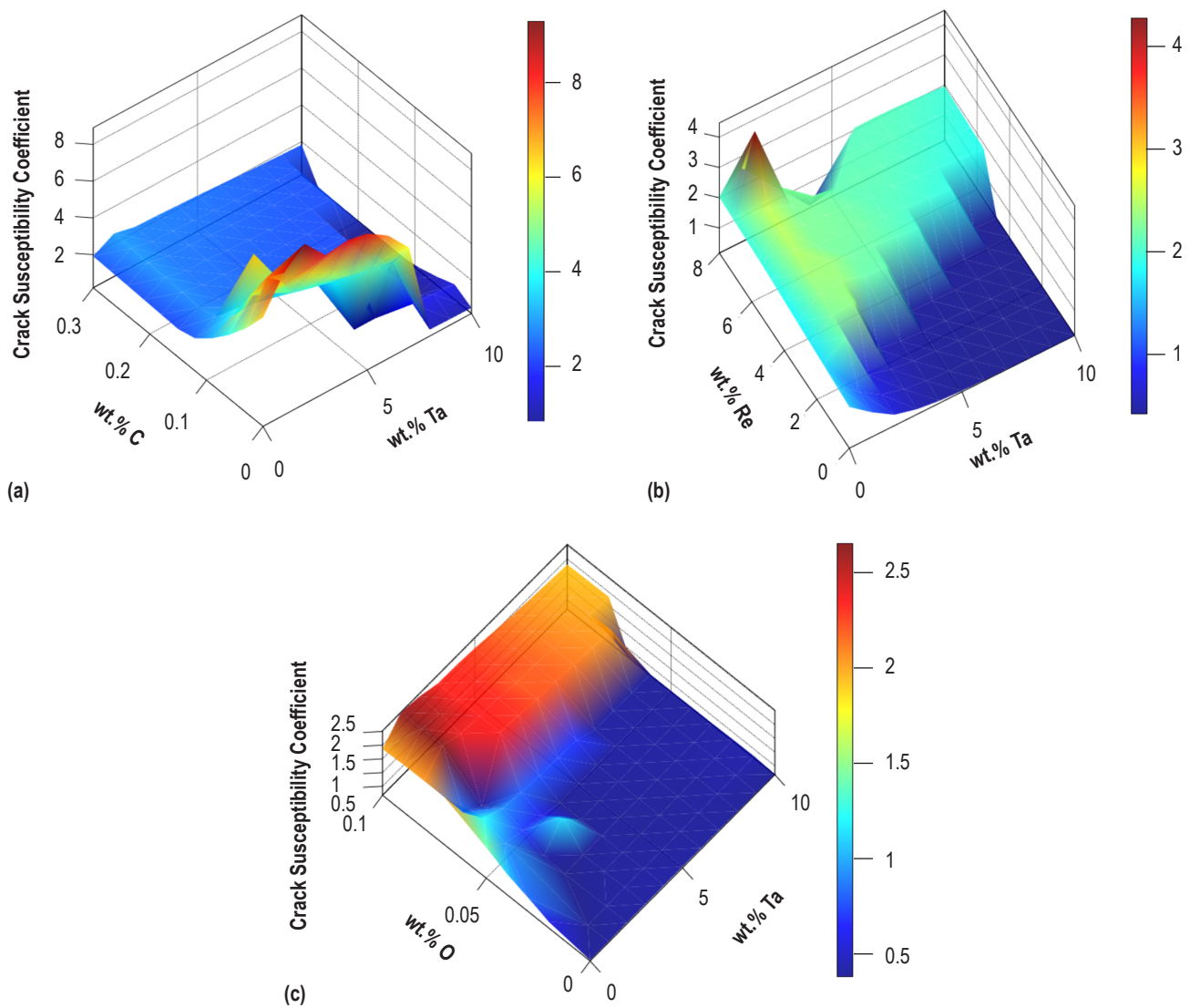

Figure 14. The CSC indices for (a) W-Re5.5-Ta-C with varied wt.% of Ta and C; (b) W-Re Ta-C0.3-O0.075 with varied wt.% of Re and TA; and (c) W-Re5.5-Ta-C0.3-O with varied wt.% of Ta and O.

With O present, the addition of C is clearly reducing the cracking susceptibility, even in models where Re is reduced to smaller amounts (yet still sufficient to enhance ductility) and models with increased wt.% of Ta. The C and O interaction should be examined further. In an upcoming TM, the authors plan to apply Thermo-Calc PRISMA solidification modeling to these issues.

For the purposes of this research, the CSC index for a system of W-R5.5-Ta5-C-O with varying amounts of C and O has been calculated via the Thermo-Calc vulnerability time method in figure 15. Again, it is seen that the assumed O content is being somewhat scavenged by getter C. These figures suggest the increase of additional C can provide realistic O impurity containment, even as C also serves to enhance desirable in-situ MC production with the previously discussed benefits such as grain refinement and ductility enhancement.
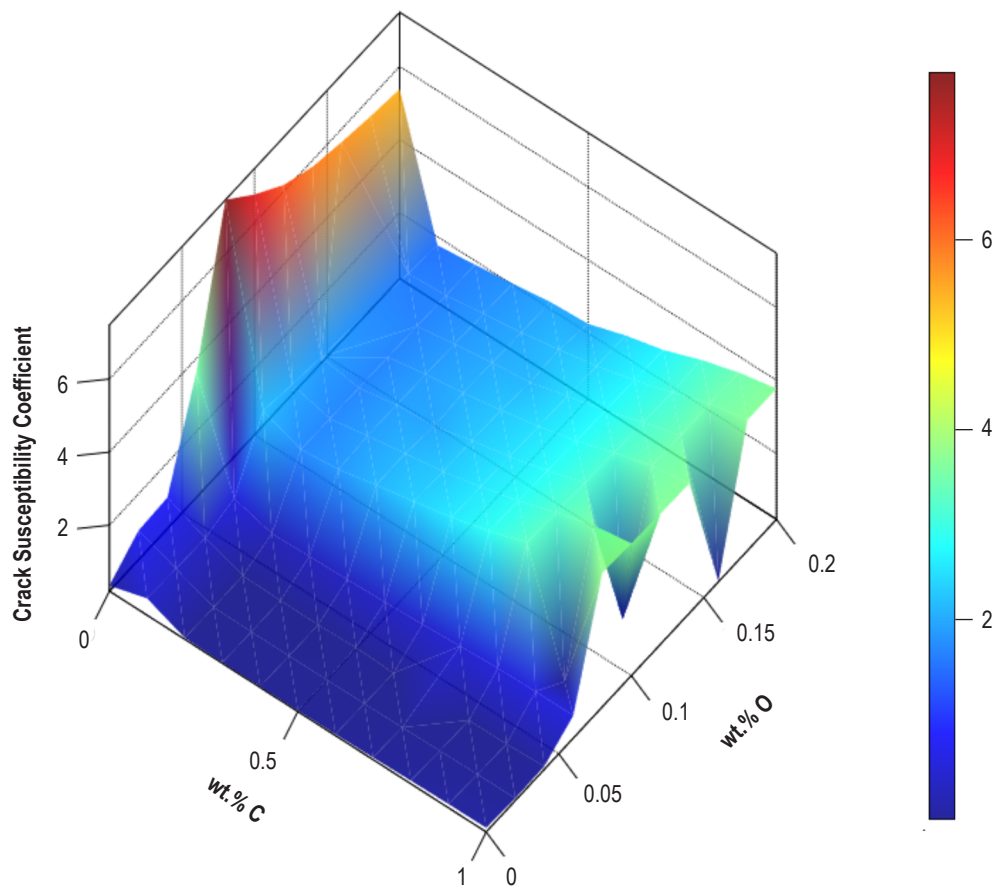

Figure 15. The CSC index for varied wt.% of C and O for the W-R5.5-Ta5-C-O system.

4. CONCLUSIONS

This TM has discussed CALPHAD calculations W-based refractory alloys, starting with a basic W-Re alloy and expanding to the more complex W-Re-Ta-C-O system as added nanoparticles are assumed to partially or fully melted.

The addition of these nanoparticles has shown some Scheil cracking suppression advantages in the $>0.95 f_s$ region, as visualized by the Thermo-Calc and CALPHAD models. In the ranges calculated, the slope or gradient is steep throughout, though indications of reduced vulnerability time as well as reduced steepness in certain regions of temperature ranges are noted. Therefore, in order to suppress cracking in W-based refractory alloys, a combination of techniques is required. One or more additional elements must be added, the manufacturing processes must be modified, and survivability of added nanoparticles must be assured in order to achieve significant grain refinement even into the $>0.95 f_s$ region, because thermal expansion and contraction occurs as liquid alloy is depleted in this critical temperature region. This combination of techniques translates to three observed improvements in the refractory alloy AM process: 1) Scheil curve flattening at the $>0.95 f_s$ region; 2) decreased temperature range in the $>0.95 f_s$ region; and 3) pair-wise decrease of the cracking susceptibility via the vulnerability time method in Thermo-Calc.

This TM discusses challenges to optimal refractory alloys AM, which are being overcome by NASA and partners via ICME development approaches, both computational and experimental. It is assumed that nanoparticles that are added to a basic refractory alloy such as W-Re will melt near-fully or fully as part of the AM process. The existence of O impurities, which are ubiquitous in AM, and the addition of a getter such as C, are also assumed as part of this research. The authors therefore conclude the following two points:

(1) The nanoparticles will mostly or melt fully under the refractory AM build conditions.

(2) The disassociated and then fully melted nanoparticles contribute as elemental atomic additions to the melt-pool. That is, an example W-Re-TaC system will behave as a W-Re-Ta-C system.

The survivability of nanoparticle additions will depend crucially on static or feedback melt-pool temperature control—that is, if within the melt temperature windows between the base metal or so-called 'parent metal' and nanoparticle, it will be useful for the nanoparticles to remain intact for simultaneous strength and ductility enhancement. If not, the nanoparticles will melt and then in-situ alloying and nanoparticle inclusion formation will take over, as discussed in this TM. The authors have calculated various compositions' solidification(s) via CALPHAD as a basis for in-situ alloying and the effects of impurities, nano-additions and even getters towards both MC and MO in-situ formation. This research has provided insight into crack free refractory alloys build optimization, both in this work and in other works yet to be published.

- A trend has been seen toward the following desired features for both ideal alloying as well as realistic AM of alloys. When C is added to alloy systems, the C presents a promising way to getter oxygen impurities via the creation of CO. In addition, C provides a source for affine in-situ MC formation, preferentially with the secondary elements rather than the parent metal of W. These in-situ formed MC inclusions will be in the nanometer scale, yet they will provide equiaxed grain refinement as well as potentially grain pinning and thermal stability.

- Additional ODs as well as cellular structures are formed via MO in-situ formation. These are not survivable in W melts, as the melt temperatures are usually on the order of the melting temperature of W itself and no process window exists. However, O scavenging toward MO formation is possible during the solidification process, which removes O impurities and thus prevents unwanted brittle phases that can lead to cracking.

- In a separate independent project, the authors have researched molybdenum (Mo)-C AM alloying and have been able to create crack-free AM parts with 0.3 wt.% of C. An additional project with NASA partners is in writing by the authors, in which a W-X-C-O system is being processed via PBF-SLM AM and is achieving crack-free AM with no base plate or substrate heating. Both of these project reports are currently in writing, but are mentioned here in support of this TM, as insights gathered from the modeling being reported here drove some of the insights that have led to such AM results under the ICME efforts of NASA MSFC and various partners.

- In the near future, the authors will publish the results of the CALPHAD analysis of the independent research into Mo-C0.3 AM of crack free parts, revisiting the experimental results from the point of view of the CALPHAD modeling and will compare those results with the full CALPHAD analysis of the crack free W-X-C-O AM predictive modeling by NASA and its partners. The modeling will further be augmented by Thermo-Calc PRISMA solidification modeling, which helped quantify the solidification production of in-situ compounds.

REFERENCES

1. Thermo-Calc Software AB: "Thermo-Calc Diffusion Module (DICTRA) Documentation Set," No. 2023a, <https://thermocalc.com/wp-content/uploads/Documentation/Current_Static/diffusion-module-dictra-documentation-set.pdf>, December 15, 2022.

2. Schwartzberg, F. R.; Ogden, H. R.; and Jaffee, R. I.: "DUCTILE-BRITTLE TRANSITION IN THE REFRACTORY METALS," Report Number DMIC-114; AD-216526; PB-151070, Defense Metals Information Center, Columbus, OH, https://catalog.hathitrust.org/Record/102326544, December 31, 1959.

3. Nieh, T. G.; and Wadsworth, J.: "RECENT ADVANCES AND DEVELOPMENTS IN REFRACTORY ALLOYS," UCRL-JC-116U7, *Materials Research Society Online Proceedings Library,* https://www.osti.gov/servlets/purl/10131865, November, 1993.

4. El-Genk, M. S.; and Tournier, J-M.: "A review of refractory metal alloys and mechanically alloyed-oxide dispersion strengthened steels for space nuclear power systems," *Journal of Nuclear Materials,* Vol. 340, No. 1, pp. 93–112, doi:10.1016/j.jnucmat.2004.10.118, April, 2005.

5. Barnes, M. W.; Tucker, D. S.; Hone, L.; and Cook, S.: "Nuclear Rocket Ceramic Metal Fuel Fabrication Using Tungsten Powder Coating and Spark Plasma Sintering," NASA/TP-2017-218236, https://ntrs.nasa.gov/citations/20170005531, April 1, 2017.

6. Volz, M. P.; Wilkerson, R.; Williams, J.; et al.: "Hot Hydrogen Testing of Carbides Developed for Nuclear Thermal Propulsion," presented at the 45th International Conference and Exposition on Advanced Ceramics, Virtual, https://ntrs.nasa.gov/citations/20210000359, January 12, 2021.

7. Mireles, O.: "Additive Manufacture of Refractory Metals for Aerospace Applications," presented at the AIAA Propulsion & Energy 2021 Forum, Virtual, https://ntrs.nasa.gov/citations/20210018657, July 14, 2021.

8. Vrancken, B.; King, W. E.; and Matthews, M. J.: "In-situ characterization of tungsten microcracking in Selective Laser Melting," in *Procedia CIRP,* September 3–6, 2018, Vol. 74, Fürth, Germany, pp. 107–110, doi:10.1016/j.procir.2018.08.050, 2018.

9. Hu, Z.; Zhao, Y.; Guan, K.; et al.: "Pure tungsten and oxide dispersion strengthened tungsten manufactured by selective laser melting: Microstructure and cracking mechanism," *Additive Manufacturing,* Vol. 36, Article 101579, doi:10.1016/j.addma.2020.101579, December, 2020.

10. Chen, J.; Zhao, C.; Li, K.; et al.: "Effect of TaC addition on microstructure and microhardness of additively manufactured tungsten," *Journal of Alloys and Compounds,* Vol. 897, Article 162978, doi:10.1016/j.jallcom.2021.162978, March 15, 2022.

11. Li, K.; Wang, D.; Xing, L.; et al.: "Crack suppression in additively manufactured tungsten by introducing secondary-phase nanoparticles into the matrix," *International Journal of Refractory Metals & Hard Materials,* Vol. 79, pp. 158–163, doi:10.1016/j.ijrmhm.2018.11.013, February 2019.

12. Wei, S.-Y.; Ji, L.-N.; Wu, W.-J..; and Ma, H.-L.: "Selective laser melting of lanthanum oxidereinforced tungsten composites: microstructure and mechanical properties," *Tungsten,* Vol. 4, pp. 67–78, doi:10.1007/s42864-021-00127-0, December 17, 2021.

13. Zhou, Y.; Che, Y.-S.; Wang, C.; et al.: "Selective laser melting high-performance ZrC-reinforced tungsten composites with tailored microstructure and suppressed cracking susceptibility," *Tungsten,* Vol. 3, pp. 72-88, doi:10.1007/s42864-021-00076-8, March 08, 2021.

14. Thermo-Calc Software AB: "Thermo-Calc Databases," No. 2023a, < https://thermocalc.com/products/databases/> December 15, 2022.

15. Wendel, J.: "Thermodynamics and Kinetics of Tungsten Oxidation and Tungsten Oxide Sublimation in the Temperature Interval 200°–1100°C," Master's Thesis, Lund University, Lund, Sweden, 105 pp., https://lup.lub.lu.se/luur/download?fileOId=4756159&func=downloadFile&recordOId=4756155, 2014.

16. Wolverton, C.: "The Open Quantum Materials Database," Northwestern University, < https://oqmd.org/>, 2019, accessed March 15, 2023.

17. Saal, J. E.; Kirklin, S.; Aykol, M.; et al.:"Materials Design and Discovery with High-Throughput Density Functional Theory: The Open Quantum Materials Database (OQMD)", *JOM* Vol. 65, pp. 1501-1509, doi:10.1007/s11837-013-0755-4, September 28, 2013.

18. Kirklin, S.; Saal, J.E.; Meredig, B.; et al.: "The Open Quantum Materials Database (OQMD): assessing the accuracy of DFT formation energies", *npj Computational Materials,* Vol. 1, Article 15010, doi:10.1038/npjcompumats.2015.10, December 11, 2015.

19. Michael, F. N.; and Sowards, J. W.: "Numerical Study of Solidification Crack Susceptibility in Novel Refractory Alloy Systems," NASA/TM-20230002218, https://ntrs.nasa.gov/citations/20230002218, February 1, 2023.

National Aeronautics and
Space Administration
IS63
George C. Marshall Space Flight Center
Huntsville, Alabama 35812